Rotating disk flow stability in electrochemical cells: Effect of viscosity stratification

J. Pontes[a)]
Metallurgy and Materials Engineering Department/EP-COPPE, Federal University of Rio de Janeiro, P.O. Box 68505, 21941-972 Rio de Janeiro, RJ, Brazil

N. Mangiavacchi[b)]
Mechanical Engineering Department, State University of Rio de Janeiro, R. São Francisco Xavier 524, 20550-013 Rio de Janeiro, RJ, Brazil

A. R. Conceição[c)]
Metallurgy and Materials Engineering Department/EP-Federal University of Rio de Janeiro, P.O. Box 68505, 21941-972 Rio de Janeiro, RJ, Brazil

O. E. Barcia[d)]
Institute of Chemistry/IQ—Federal University of Rio de Janeiro, P.O. Box 68505, 21941-972 Rio de Janeiro, RJ, Brazil

O. R. Mattos[e)]
Metallurgy and Materials Engineering Department/COPPE-Federal University of Rio de Janeiro, P.O. Box 68505, 21941-972 Rio de Janeiro, RJ, Brazil

B. Tribollet[f)]
UPR15—CNRS, Physique des Liquides et Electrochimie, 4 place Jussieu, 75252 Paris Cedex 05, France

(Received 26 March 2003; accepted 1 December 2003; published online 4 February 2004)

This work is about the effect of viscosity stratification on the hydrodynamic instability of rotating disk flow, and whether or not it can take into account experimental observations of the lowering of critical Reynolds numbers in electrochemical systems, where a viscosity stratification is assumed to result from the gradients of chemical species existing in the convective boundary layer near the disk electrode. The analysis is for temporal stability of a class of von Kármán solutions: fully three-dimensional modes are considered and the neutral curves are therefore functions of not only the Reynolds number but also the wave frequency and the two wave numbers. Global minimization over wave numbers and also over the frequency gives the critical Reynolds number. The neutral curves exhibit a two-mode structure and the dependence of both modes on parameters is studied. It is shown that viscosity stratification leads to an increase in the range of parameters where perturbations are amplified and to a reduction of the critical Reynolds number, in a wide range of perturbation frequencies. The results support the hypothesis that the current oscillations may originate from a hydrodynamic instability. © *2004 American Institute of Physics.*
[DOI: 10.1063/1.1644147]

I. INTRODUCTION

Electrochemical cells using a rotating disk electrode are a widely used experimental tool in electrochemistry, due to the simplicity of the setup and the fact that the mass flux is independent of the radial position along the disk, at steady state conditions.[1] Furthermore, the rate of transfer of ions close of the electrode is conveniently controlled by imposing an adequate angular velocity to the electrode. This rate of transfer defines the maximum steady state current attained in an experiment.

Figure 1(a) schematically shows the setup used in practical electrochemical works.[2] It consists of a classical arrangement with a counterelectrode, a reference electrode, and a working electrode. Polarization curves experimentally obtained in the electro-dissolution of iron electrodes, using the described arrangement, present three different regions,[3] schematically shown in Fig. 1(b).

Two current instabilities are observed in the third region: one at the beginning of the plateau and a second one at the end, where the electrode surface undergoes an active to passive transition.[4] The first instability is intrinsic to the system, while the current instability close to the active–passive transition is affected by the output impedance of the control equipment. This instability can be suppressed by using a negative feedback resistance,[5] which gives rise to a continuous transition.

Most explanations presented in the literature for the current instabilities are based on mechanisms proposing a

[a)]Electronic mail: jopontes@ufrj.br
[b)]Electronic mail: norberto@uerj.br
[c)]Electronic mail: anderson@metalmat.ufrj.br
[d)]Electronic mail: barcia@metalmat.ufrj.br
[e)]Electronic mail: omattos@metalmat.ufrj.br
[f)]Electronic mail: bt@ccr.jussieu.fr

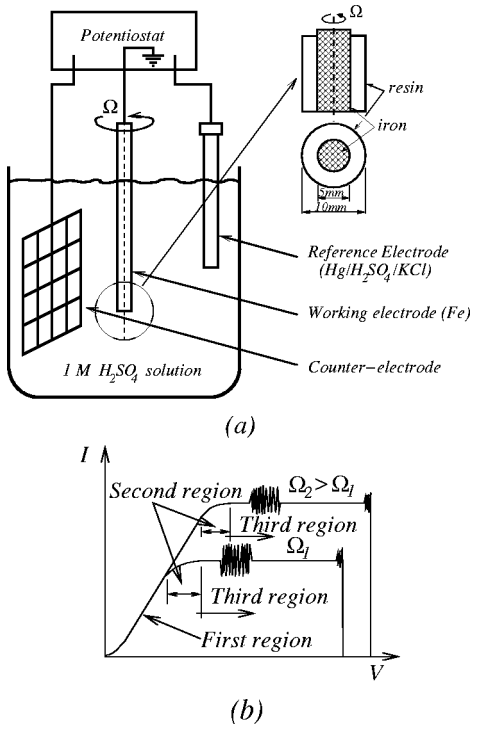

FIG. 1. The electrochemical cell and the rotating disk electrode in (a) and the polarization curves with the three regions, schematically shown in (b).

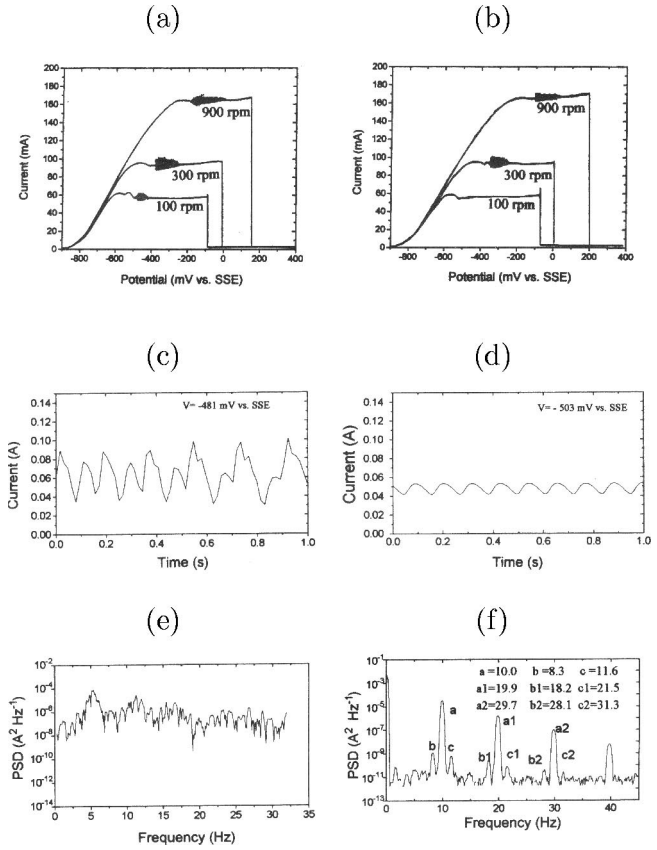

FIG. 2. Polarization curves, current time series in the instability region at the beginning of the plateau, and PSDs obtained in the electro-dissolution of iron electrodes in a 1 M H_2SO_4 solution. (a), (c), and (e): Polarization curves for an electrolyte without glycerol, current time series at 100 rpm, -523 mV, and the associated PSD, respectively. (b), (d), and (f): Same, for an electrolyte with a 1 M glycerol solution. Time series in (d) refers to the electrode turning at 300 rpm at a potential of -503 mV (from Ref. 8).

$FeSO_4$ film precipitated at the electrode surface.[6] In fact, changes in the ohmic voltage drop due to precipitation and dissolution of a $FeSO_4$ film provide an acceptable explanation for the instability observed in the active/passive transition region, coupled with the output impedance of the control equipment. However, this model cannot be generalized to explain oscillations observed at the beginning of the current plateau. Indeed, using electrohydrodynamic impedance measurements,[7] Barcia *et al.*[3] studied the electro-dissolution of iron electrodes in 1 M H_2SO_4 at the current plateau, before and after the first instability region. Barcia *et al.*[3] verified that the electrode surface is uniformly accessible before and after the first current instability, showing that the surface is not covered by a film. In these conditions it is highly improbable that the electro-dissolution kinetics leads to the deposition of a film in the beginning of the first instability region and that this film disappears at the end of that region, in order to restore the steady-state current at the same level observed before the onset of the instability. Moreover, Barcia *et al.*[3] propose that the electro-dissolution process leads to the existence of a viscosity gradient in the diffusion boundary layer, which could affect the stability of the hydrodynamic field and explain the observed current instability.

To investigate the importance of the hydrodynamics in the electro-dissolution of iron, Ferreira *et al.*[4] and Geraldo *et al.*[8] studied the influence of the viscosity on the current oscillations observed at the beginning of the current plateau region of the above described experiment. These authors found that by increasing the bulk electrolyte viscosity—and therefore decreasing the Reynolds number of the experiment—by adding glycerol to the solution, the current oscillations evolve from chaotic to periodic and to a stationary regime, where the instability is suppressed. They also found that the current oscillations are enhanced by an increase in the angular velocity of the electrode. The main results obtained by these authors are summarized in Fig. 2.

Figures 2(a) and 2(b) show the polarization curves obtained for the Fe/1 M H_2SO_4 system, at three different angular velocities of the working electrode. Figure 2(a) refers to an electrolyte without glycerol and Fig. 2(b) to a system containing a 1.0 M glycerol solution. Figures 2(c)–2(d) show current time series for the oscillations observed at 100 rpm and -523 mV in Fig. 2(a) and for the oscillations observed at 300 rpm and -503 mV in Fig. 2(b), respectively. The corresponding power spectral density (PSD) is given in Figs. 2(e)–2(f). In both configurations the current oscillations occur for a larger range of ΔV at 900 rpm than at lower angular velocities. In the case of the experiment conducted with glycerol, the current instability is suppressed at 100 rpm. In addition, oscillations observed at 100 rpm in the cell without glycerol present a chaotic behavior, as shown by the PSD, whereas oscillations at 300 rpm in the system containing glycerol are periodic.

The existence of a hydrodynamic instability in rotating disk flow has been the object of a number of investigations, both experimental and theoretical, in the case of fluids with

uniform viscosity. The main result shows that the steady flow becomes unstable beyond a certain nondimensional distance from the axis of rotation.

The flow develops corotating vortices which spiral outward with their axes along logarithmic spirals of angle $90° + \varepsilon$ ($\varepsilon \approx 13°$) with respect to the radius of the disk. The first study of transition on a rotating disk, due to Smith,[9] found sinusoidal disturbances in the boundary layer. Subsequently, Gregory *et al.*[10] found stationary vortices from a nondimensional radius $R=430$ in a flow visualization using the wet-china–clay technique. Chin and Litt[11] used an electrochemical technique to evaluate the transition region, which was found to occur between 412 and 590. The experimental critical value of R found in the literature, below which all small disturbances dampen, ranges from 182 and 530. As pointed out by Wilkinson and Malik,[12] "the discrepancy between the values of critical Reynolds number obtained from hot-wire studies and the earlier relatively high values obtained by visual techniques clearly results from the insensitivity of visual techniques to very small disturbances."

Malik[24] determined the neutral stability curve for stationary vortex disturbances, which turn with the angular velocity of the disk. The neutral curve was obtained through a linear stability analysis, in which viscosity, streamline curvature, and Coriolis force effects were taken into account. Neutral curves were presented in the $\alpha \times R$, $\beta \times R$, and $\varepsilon \times R$ planes for zero-frequency disturbances, where α and β are the components of the real perturbation wave vector along the radial and azimuthal directions and ε is the angle between the perturbation and the radial direction, given by $\varepsilon = \tan^{-1} \beta/\alpha$. The critical Reynolds number was found to be in good agreement with experimental results, at a value of $R=285.36$.

A comprehensive review of the literature on the subject, concerning research made until 1989, can be found in the paper by Reed and Saric.[13]

Faller[14] determined the neutral stability curves for setup configurations consisting of rotating or stationary disks and flows approaching the disk with (rotating flow) or without (stationary flow) bulk angular velocity. Critical Reynolds number for the case of rotating disk and stationary fluid was found to be 69.4.

Lingwood[15] presented the neutral curve for vortices turning with several angular velocities and theoretical results concerning the asymptotic response of the flow to an impulsive excitation exerted in the flow at a certain radius at $t=0$. Additionally, Lingwood's work addresses the case where the wave number component along the radial direction, α, is complex, leading to an exponential growth along that direction. The curve for this case defines the region of absolute instability, with a critical Reynolds number of $R=510.625$.

It is well known that boundary layers can be destabilized by increasing the viscosity close to the wall and stabilized by decreasing, through heating or cooling the wall.[16] Schäfer *et al.*[17] deduced an asymptotic expression for the critical Reynolds number for moderate temperature differences in boundary layers developed over flat plates, taking into account the temperature dependence of the viscosity. Turkyilmazoglu *et al.*[18] studied the influence of heat transfer on the convective and absolute instability of compressible boundary layers in rotating disk flow.

The main purpose of the present paper is to use the empirical viscosity profile assumed by Barcia *et al.*[3] and to verify through a linear stability analysis if the viscosity stratification can give rise to the current oscillations observed by the authors and summarized above.

It is clear that this empirical profile can only be justified by the concentration gradient of the relevant chemical species existing close to the electrode surface. Consequently, the model developed in the present paper is only a first qualitative step trying to take into account the main experimental results, previously outlined. A complete model coupling hydrodynamics and the mass transport equations is now in progress, aiming to quantitatively describe the results.

In spite of the importance of absolute instabilities in the transition to turbulence we restrict ourselves to the study of the neutral curve of convective instabilities that represent the lowest limit below which no small disturbances are amplified.[19]

The paper is organized as follows: Section II describes the steady velocity flow, which is the problem base state, for the case of constant viscosity fluids and for four viscosity profiles configurations assumed in this work. Section III deals with the linearized equations of the perturbed flow. Section IV presents and discusses the results and the conclusions are summarized in Sec. V. Appendix A deals with derivation of the disturbance evolution equations and a short discussion of the numerical procedures is given in Appendix B.

II. THE BASE STATE

The steady hydrodynamic field is the well known von Kármán[20] exact solution of the continuity and Navier–Stokes equations for laminar rotating disk flow, written in a rotating coordinate frame turning with the disk angular velocity Ω.

$$\mathbf{div}\,\mathbf{v}=0,$$

$$\frac{D\mathbf{v}}{Dt}=-2\boldsymbol{\Omega}\times\mathbf{v}-\frac{1}{\rho}\mathbf{grad}\,p+\frac{1}{\rho}\mathbf{div}\,\tau,$$

where $-2\boldsymbol{\Omega}\times\mathbf{v}=2\Omega(v_\theta \mathbf{e_r}-v_r\mathbf{e_\theta})$ and τ is the viscous stress tensor for a Newtonian fluid with the viscosity μ depending on the axial coordinate z. The components of stress tensor are given by[16]

$$\tau_{rr}=2\mu\frac{\partial v_r}{\partial r},$$

$$\tau_{\theta\theta}=2\mu\left(\frac{1}{r}\frac{\partial v_\theta}{\partial\theta}+\frac{v_r}{r}\right),$$

$$\tau_{zz}=2\mu\frac{\partial v_z}{\partial z},$$

$$\tau_{r\theta}=\tau_{\theta r}=\mu\left(r\frac{\partial}{\partial r}\left(\frac{v_\theta}{r}\right)+\frac{1}{r}\frac{\partial v_r}{\partial\theta}\right),$$

$$\tau_{\theta z}=\tau_{z\theta}=\mu\left(\frac{\partial v_\theta}{\partial z}+\frac{1}{r}\frac{\partial v_z}{\partial\theta}\right),$$

$$\tau_{rz}=\tau_{zr}=\mu\left(\frac{\partial v_r}{\partial z}+\frac{\partial v_z}{\partial r}\right).$$

The steady solution takes the form

$$\overline{v_r}=r\,\Omega\,F(\xi), \tag{1}$$

$$\overline{v_\theta}=r\,\Omega\,G(\xi), \tag{2}$$

$$\overline{v_z}=(\nu(\infty)\Omega)^{1/2}H(\xi), \tag{3}$$

$$\overline{p}=\rho\,\nu(\infty)\Omega P(\xi), \tag{4}$$

where $\xi=z(\Omega/\nu(\infty))^{1/2}$ and $\nu(\infty)$ is the bulk viscosity, far from the electrode surface. Equations (1)–(4) are introduced in the dimensional continuity and Navier–Stokes equations, leading to the following system of equations for F, G, H, and P:

$$2F+H'=0, \tag{5}$$

$$F^2-(G+1)^2+HF'=\frac{d}{d\xi}\left(\frac{\nu(\xi)}{\nu(\infty)}F'\right), \tag{6}$$

$$2F(G+1)+HG'=\frac{d}{d\xi}\left(\frac{\nu(\xi)}{\nu(\infty)}G'\right), \tag{7}$$

$$P'+HH'=2\frac{\nu'(\xi)}{\nu(\infty)}H'+\frac{\nu(\xi)}{\nu(\infty)}H''. \tag{8}$$

Boundary conditions for F, G, and H are $F=H=P=G=0$, when $\xi=0$, $F=H'=0$, $G=-1$ when $\xi\to\infty$. In order to integrate Eqs. (5)–(8) a viscosity profile must be assumed. In this work we use the following profile proposed by Barcia *et al.*:[3]

$$\frac{\nu(\xi)}{\nu(\infty)}=\frac{\nu(0)}{\nu(\infty)}+\left(1-\frac{\nu(0)}{\nu(\infty)}\right)\frac{q^{1/3}}{\Gamma(4/3)}\int_0^\xi e^{-q\xi^3}d\xi. \tag{9}$$

The parameter q defines the slope of the viscosity profile close to the electrode surface. This viscosity profile follows a law similar to the one of the concentration profile of Fe^{2+}, which is produced at the interface by the electrodissolution.[21]

Figure 3 shows the nondimensional viscosity and velocity profiles obtained by numerical integration of Eqs. (5)–(8) and used in the stability analysis presented in this work. Viscosity profiles with $q=2.0$ result in a decay of the viscosity to the bulk value at $\xi=1.0$ approximately. The velocity components are not too affected by the viscosity profile. A decrease in the slope of the viscosity profiles obtained with $q=0.25$ increases the deviation of the velocity profiles from the constant viscosity case and affects the incoming mass flow rate.

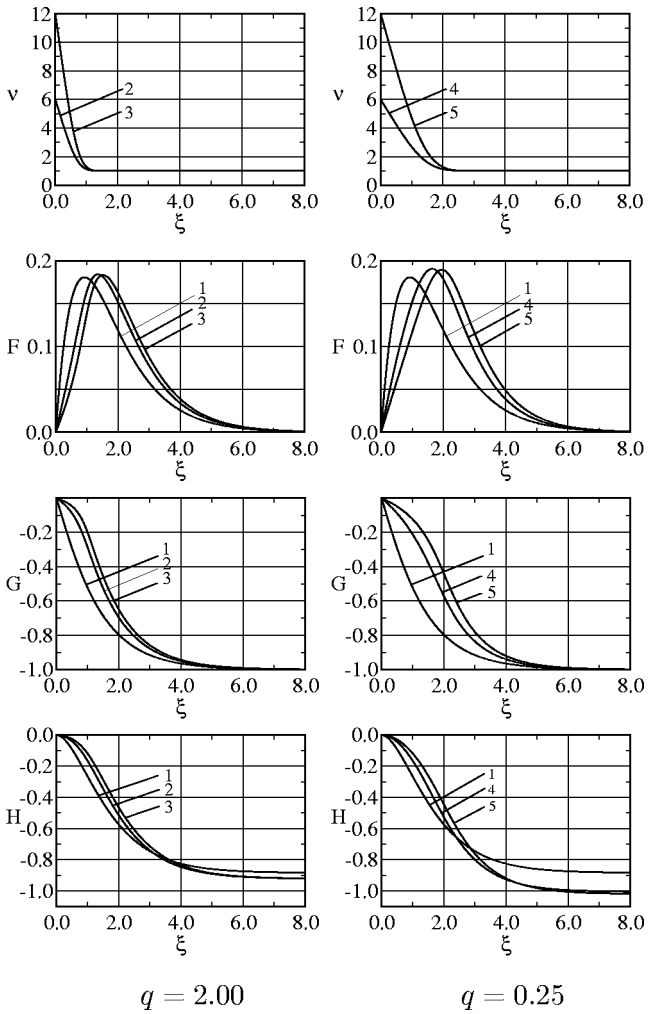

FIG. 3. Dimensionless viscosity, ν, and velocity profiles F, G, and H. (Curves No. 1) Constant viscosity fluids. (Curves Nos. 2 and 3) Variable viscosity fluids with $\nu(0)/nu(\infty)=6$ and $\nu(0)/nu(\infty)=12$, respectively, and $q=2$. (Curves Nos. 4 and 5) Variable viscosity fluids with $\nu(0)/nu(\infty)=6$ and $\nu(0)/nu(\infty)=12$, respectively, and $q=0.25$ [see Eq. (9)].

III. PERTURBATIONS OF THE BASE STATE

We turn now to the question of the stability of the steady configurations of the hydrodynamic field described in Sec. II, with respect to infinitesimally small disturbances. Variables are made nondimensional as follows: radial and axial coordinates are divided by the reference length $(\nu(\infty)/\Omega)^{1/2}$, velocity components are divided by the reference velocity $r_e^*\Omega$, pressure is divided by the reference pressure $\rho(r_e^*\Omega)^2$, viscosity is divided by the bulk value $\nu^*(\infty)$, and time and the eigenvalue of the linearized problem are divided by the time required by a particle, turning with the azimuthal velocity $r_e^*\Omega$, to move a distance equal to the reference length $(\nu(\infty)/\Omega)^{1/2}$. Here, r_e^* is the dimensional coordinate along the radial direction where the stability analysis is made. We define also the Reynolds number by the relation

$$R=r_e^*\left(\frac{\Omega}{\nu(\infty)}\right)^{1/2}. \tag{10}$$

The perturbed nondimensional velocity components and pressure are written as

$$v_r(t,r,\theta,\xi)=\frac{r}{R}F(\xi)+\tilde{v}_r(t,r,\theta,\xi), \tag{11}$$

$$v_\theta(t,r,\theta,\xi)=\frac{r}{R}G(\xi)+\tilde{v}_\theta(t,r,\theta,\xi), \tag{12}$$

$$v_z(t,r,\theta,\xi)=\frac{1}{R}H(\xi)+\tilde{v}_z(t,r,\theta,\xi), \tag{13}$$

$$p(t,r,\theta,\xi)=\frac{1}{R^2}P(\xi)+\tilde{p}(t,r,\theta,\xi), \tag{14}$$

with perturbation given by

$$\begin{pmatrix}\tilde{v}_r\\ \tilde{v}_\theta\\ \tilde{v}_z\\ \tilde{p}\end{pmatrix}=\begin{pmatrix}f(\xi)\\ g(\xi)\\ h(\xi)\\ \pi(\xi)\end{pmatrix}\exp[i(\alpha r+\beta R\theta-\omega t)], \tag{15}$$

where ω is a complex number, with $\mathcal{R}(\omega)$ and $\mathcal{I}(\omega)$ being, respectively, the frequency and the rate of growth of the perturbation. Parameters α and β are the components of the perturbation wave vector along the radial and azimuthal directions. For a given time, the phase of the perturbation is constant along branches of a logarithmic spiral, with the branches curved in the clockwise direction if β/α is positive and counterclockwise, if negative. The structure turns counterclockwise if ω/β is positive and clockwise, if negative.

Perturbation variables are introduced in the nondimensional continuity and Navier–Stokes equations, together with the parallel flow hypothesis, in order to confirm the assumption that perturbation variables are separable. To conclude, terms of order R^{-2} are dropped, leading to

$$\begin{pmatrix}a_4D^4+a_3D^3+a_2D^2+a_1D+a_0; & b_1D+b_0\\ c_1D+c_0; & d_2D^2+d_1D+d_0\end{pmatrix}\begin{pmatrix}h\\ \eta\end{pmatrix}=\omega\begin{pmatrix}q_2D^2+q_0; & 0\\ 0; & s_0\end{pmatrix}\begin{pmatrix}h\\ \eta\end{pmatrix} \tag{16}$$

with the coefficients given by

$$a_4=i\nu,\quad a_3=i(2\nu'-H),$$

$$a_2=i\nu''-i\nu(\lambda^2+\overline{\lambda^2})+R(\alpha F+\beta G)-i(H'+F),$$

$$a_1=-i\nu'(\lambda^2+\overline{\lambda^2})+iH\overline{\lambda^2},$$

$$a_0=i\overline{\lambda^2}(\nu''+\nu\lambda^2)-R(\alpha F+\beta G)\overline{\lambda^2}-R(\overline{\alpha}F''+\beta G'')+iH'\overline{\lambda^2},$$

$$b_1=2(G+1),\quad b_0=2G',$$

$$c_1=2(G+1),\quad c_0=-iR(\alpha G'-\beta F'),$$

$$d_2=i\nu,\quad d_1=i(\nu'-H),$$

$$d_0=-i\nu\lambda^2+R(\alpha F+\beta G)-iF,$$

$$q_2=R,\quad q_0=-R\overline{\lambda^2},\quad s_0=R.$$

Further details concerning the derivation of Eq. (16) are given in Appendix A.

Boundary conditions of the problem require nonslip flow and vanishing axial component of the velocity at the electrode surface. These conditions are already fulfilled by the base state, so the hydrodynamic field cannot be modified by the perturbation at the electrode surface. Consequently, we must require $g=h=0$ in $\xi=0$. Moreover, we conclude from Eq. (A5) that $h'=0$ at the electrode surface. In $\xi\to\infty$ we require that the perturbation vanishes $(g=h=0)$ and that $h'=0$.

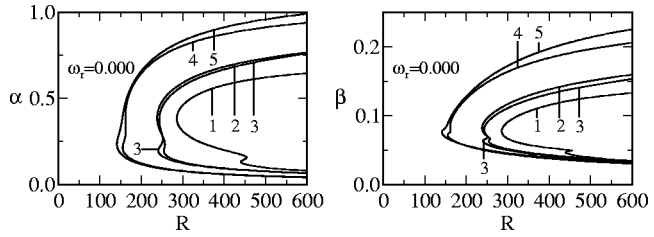

FIG. 4. Neutral curves in the planes $R\times\alpha$ and $R\times\beta$ for stationary disturbances $(\omega_r=0)$. (Curves No. 1) Constant viscosity fluids. (Curves Nos. 2–5) The four variable viscosity cases.

Equation (16) defines a generalized eigenvalue/eigenfunction problem. The eigenfunctions are the normal modes of the model, with the imaginary and real parts of each eigenvalue being, respectively, the rate of growth and the angular velocity of the perturbation relative to the angular velocity of the disk.

For a given viscosity profile the parameter space of the problem contains three variables: the Reynolds number and the perturbation wave vector components α and β.

IV. RESULTS

The effect of viscosity stratification is analyzed by comparing stability properties of constant viscosity fluids with the properties of the four variable viscosity configurations discussed in Sec. II.

The results are summarized in Figs. 4–9. Figures 4–6 show the neutral stability curves, a plot of the growth rates of two modes is given in Fig. 7, and Figs. 8 and 9 present a plot

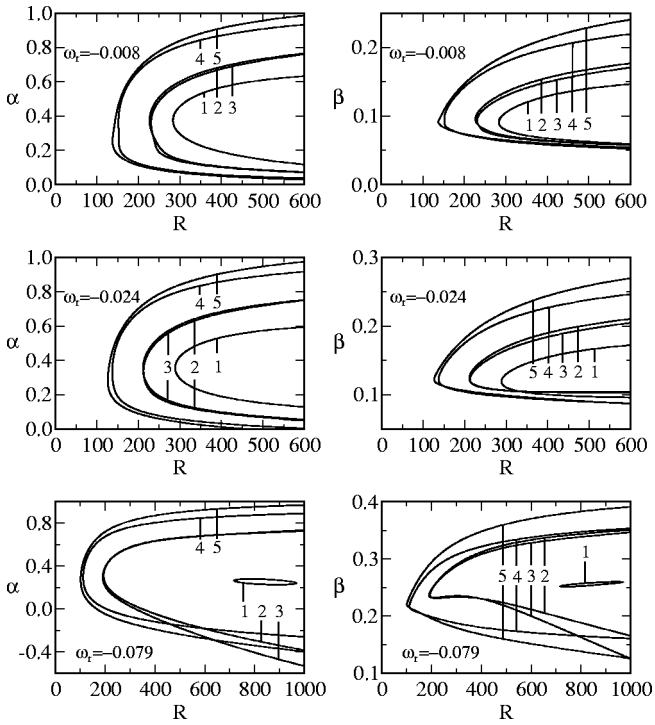

FIG. 5. Neutral curves in the planes $R\times\alpha$ and $R\times\beta$ for negative values of ω_r. (Curves No. 1) constant viscosity fluids. (Curves Nos. 2–5) The four variable viscosity cases.

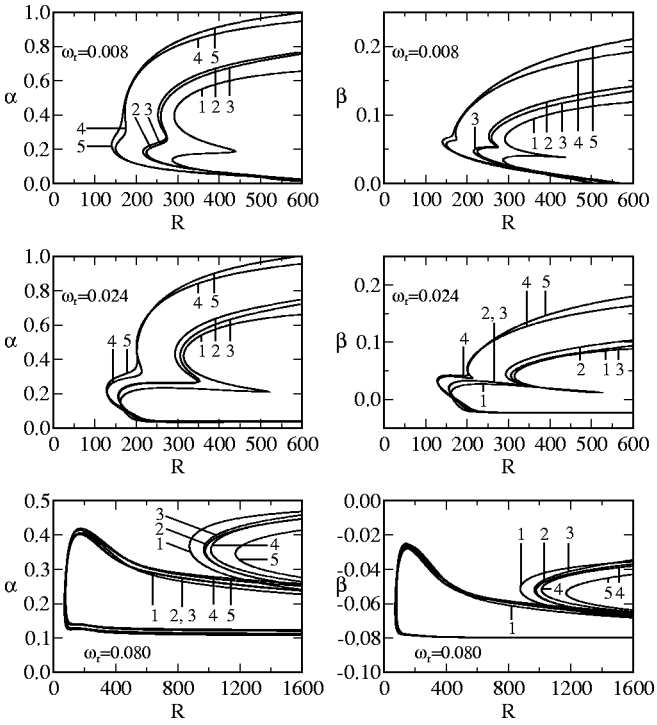

FIG. 6. Neutral curves in the planes $R\times\alpha$ and $R\times\beta$ for positive values of ω_r. (Curves No. 1) Constant viscosity fluids. (Curves Nos. 2–5) The four variable viscosity cases.

of the critical Reynolds number, the associated wave number, and the spiral angle, as functions of the perturbation frequency ω_r.

The neutral curves (Figs. 4–6) exhibit a two-branch structure, showing that two different modes become unstable in the range of Reynolds and perturbation wave numbers covered in this work. One of the modes is strongly destabilized by the viscosity stratification and has a rate of growth 1 order of magnitude higher than the second one (see Fig. 7), in its unstable region. Nevertheless, this mode is not the most unstable. The most unstable mode is less affected by the viscosity stratification. The behavior of the most unstable modes as a function of the perturbation frequency summarizes the main results of this work (Figs. 8 and 9).

The neutral curves were evaluated in domains with length $\xi_{\max}=50$, using grids with 1001 uniformly spaced points. Larger domains do not significantly affect the presented results. Values specified for ω_r are -0.079, -0.024, -0.008, 0.000, 0.008, 0.024, and 0.080. Curves No. 1 in Figs. 4–6 refer to constant viscosity fluids, the remaining ones to variable viscosity fluids: Curves Nos. 2 and 3 refer to fluids with $\nu(0)/\nu(\infty)=6.0$ and $\nu(0)/\nu(\infty)=12.0$, respectively, both with $q=2.00$. Curves Nos. 4 and 5 refer to fluids with $\nu(0)/\nu(\infty)=6.0$ and $\nu(0)/\nu(\infty)=12.0$, respectively, both with $q=0.25$.

Curves relative to stationary disturbances ($\omega_r=0$) are shown in Fig. 4 and represent an extension of Malik's work, by including the variable viscosity cases. Figure 5 presents neutral curves with $\omega_r<0$. Since β is always positive in this case, the neutral curves shown in this figure refer to distur-

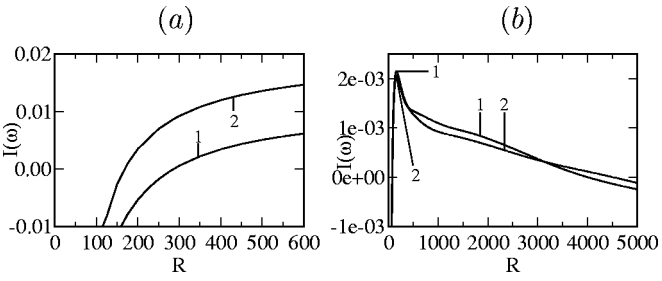

FIG. 7. Rate of growth, $\mathcal{I}(\omega)$, of perturbations, as a function of the Reynolds number, R, for constant (curves No. 1) and a variable viscosity with $\nu(0)/\nu(\infty)=6$, $q=0.25$ (curves No. 2): (a) $\alpha=0.38381$ and $\beta=0.077\,42$; (b) $\alpha=0.1934$ and $\beta=-0.063\,43$.

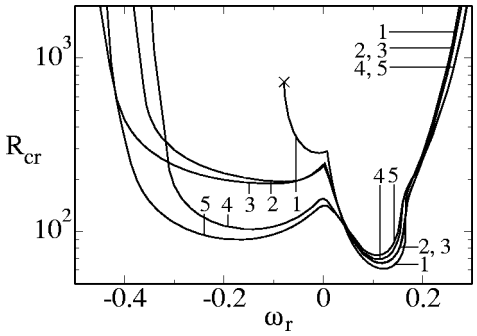

FIG. 8. Absolute minima $R_{\rm cr}$, as a function of the perturbation frequency ω_r for modes 1 and 2. (Curves No. 1) Constant viscosity fluids. (Curves Nos. 2–5) The four variable viscosity cases. The point marked by a cross ($\times$) in curve No. 1 identifies the limit frequency, ω_r, below which all perturbations for the constant viscosity case are damped.

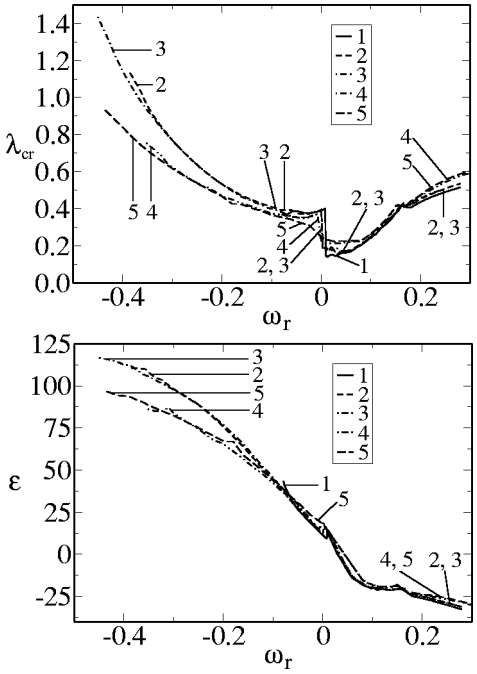

FIG. 9. (Top) Critical wave number, $\lambda_{\rm cr}=(\alpha^2+\beta^2)^{1/2}$, as a function of the perturbation frequency ω_r. (Bottom) Spiral angle, $\varepsilon=\tan^{-1}\beta/\alpha$ (degrees), of the critical wave vector, as a function of the perturbation frequency ω_r. (Curves No. 1) Constant viscosity fluids. (Curves Nos. 2–5) The four variable viscosity cases.

bances turning slower than the disk. Figure 6 contains neutral curves built for $\omega_r > 0$.

Most neutral curves presented in Figs. 4–6 have two minima (one located in an upper branch, the other one in a lower branch) and the branches are affected differently by the parameters of the viscosity profile and by ω_r.

The level of reduction in the critical Reynolds number of a neutral curve depends on ω_r. At the upper extreme of values, $\omega_r = 0.080$ (lower line in Figs. 6 and 8), variable viscosity actually renders the flow more stable. The absolute minimum appears in the lower branch and this branch is not significantly affected when variable viscosity is introduced. In fact, even a small increase in the critical Reynolds number occurs in this case. The upper branches of the neutral curves are more affected by variable viscosity, but in the sense of rendering the flow more stable. So we conclude that variable viscosity stabilizes the flow for $\omega_r = 0.080$.

As ω_r diminishes, this effect is inversed and viscosity stratification destabilizes the flow, with the unstable region in the parameters space being enlarged and starting at lower values of the Reynolds number. Reductions in the critical Reynolds number for stationary disturbances ($\omega_r = 0$) are on the order of 50% (see Fig. 4).

Another interesting phenomenon occurs for variable viscosity flows, where the neutral stability curve crosses the value $\alpha = 0$ for $\omega_r < -0.024$. This means that, in contrast with constant viscosity flows, radial disturbances may be amplified in variable viscosity configurations.

Furthermore, at the lower extreme of values of $\omega_r(-0.079)$, the neutral curve for constant viscosity fluids almost disappears, whereas the unstable regions for variable viscosity are larger and have lower Reynolds number than regions found for higher values of ω_r. A limit close to $\omega_r = -0.079$ exists thus, below which disturbances in constant viscosity fluids are always damped. The unstable region for stratified viscosity cases extends to much lower values of ω_r and comprises negative values of α, opening the possibility of waves to propagate upstream, towards the disk axis. We conclude from Figs. 4–6 that variable viscosity not only decreases the flow stability in a wide range of values of ω_r, but also, that there are large regions in the parameters space where the flow is unstable under variable viscosity and otherwise stable under constant viscosity.

We discuss now the influence of the two parameters $\nu(0)/\nu(\infty)$ and q of the viscosity profiles [Eq. (9)], on the neutral curves. Figures 4–6 show that the main factor affecting the critical Reynolds number of a neutral curve is the parameter q [Eq. (9)], which defines the thickness of the layer in which the viscosity varies. As a rule, thicker layers lead to larger reductions, except in the extreme case of $\omega_r = 0.080$. The above results are, qualitatively, in agreement with the experimental ones. Indeed, as shown in Fig. 2, the system becomes more unstable as the angular velocity of the electrode increases, and more stable as the bulk viscosity increases, with addition of glycerol.

The effect of the ratio $\nu(0)/\nu(\infty)$ on the neutral curves is less important and not so well defined. It leads to reductions in the critical Reynolds number in some cases, and to increases in other cases. For instance, if stationary disturbances are considered ($\omega_r = 0$), an increase in $\nu(0)/\nu(\infty)$ from 6 to 12, setting $q = 2$, slightly reduces the critical Reynolds number, whereas the opposite effect is observed with $q = 0.25$.

Figure 7 shows the effect of the Reynolds number on the rate of growth of mode 1 perturbations [Fig. 7(a)] and mode 2 [Fig. 7(b)], for constant viscosity and one case of variable viscosity, showing that the most unstable modes (modes 2) have a much lower rate of growth at large Reynolds numbers.

On one hand, Fig. 7(b) shows that modes 2 are the result of a viscous instability, having maximum rate of growth at a finite Reynolds number and becoming more and more stable as the R increases. Hence, these modes rely on the existence of viscous effects to be amplified. It should be pointed out that modes 2 extend to large distances from the disk surface. This is due to the fact that h decays as $h \rightarrow e^{-\lambda \xi}$ for large values of ξ and that λ for modes 2 is typically two times smaller than for modes 1. Therefore, the length of modes 2 is much larger than the length scale where the viscosity gradient exists. This may explain the fact that the viscosity stratification has a rather small influence on the growth rate of modes 2.

On the other hand, Fig. 7(a) shows that modes 1 result from an inviscid instability, since the growth rate monotonically increases with the Reynolds number. Furthermore, the variable viscosity growth rate is always higher than the one of the constant viscosity configuration, showing evidence that the viscosity stratification affects the flow stability through the deviation introduced on the base flow velocity profiles, rather than through viscous instability mechanisms.

The effect of variable viscosity on the critical Reynolds number of modes 1 and 2 is summarized in the plot of $R_{cr} \times \omega_r$, presented in Fig. 8, which shows the existence of amplified perturbations in variable viscosity fluids, for a much larger range of negative values of ω_r, than in constant viscosity ones.

The upper branch shows a plateau at small absolute values of ω_r, and moves to much higher Reynolds numbers for high absolute values of ω_r in the case of constant viscosity fluids (see Fig. 8). For the variable viscosity cases, the curve shows a much wider plateau that extends to more negative values of ω_r.

The lower branch of the neutral curves is affected in a different way by ω_r. At $\omega_r = -0.079$ only the upper branch appears in the diagrams of the neutral curves. As ω_r increases the lower branch appears, moves to lower Reynolds numbers, and the critical Reynolds number of the entire neutral curve is eventually placed in this branch. By further increasing ω_r an absolute minimum Reynolds number is attained. After that point the critical Reynolds number rapidly increases.

It is worth noting that the absolute minimum of a neutral curve built for a given value of ω_r occurs in the upper branch and, in some cases, in the lower branch when the viscosity profile changes. This is the case, for instance, of the neutral curves drawn for stationary disturbances ($\omega_r = 0.000$), where

the minimum associated to the lower branch occurs at a substantially higher value of the Reynolds number than the absolute minimum, for constant viscosity fluids. When variable viscosity is considered both branches have approximately the same R_{cr} with $q=2.0$ [see Eq. (9)] and the absolute minimum occurs in the lower branch for $q=0.25$.

Figure 9 shows plots of the critical wave numbers and spiral angle, as functions of frequency. Stratified viscosity results in a wider range of unstable wave numbers than in the constant viscosity case. A discontinuous change in the curve occurs at the switch between critical modes, except for the case $\nu(0)/\nu(\infty)=12$, $q=0.25$, where the transition is smooth.

A larger unstable range of spiral angles is also observed for stratified viscosity cases. The angle basically decreases monotonically with ω_r. The maximum angle is less than 50° for constant viscosity and extends to more than 90° in the stratified configurations, opening up the possibility of the existence of radial structures and of waves propagating upstream, as mentioned before. The discontinuity at the mode switching, though not so strong as in the wave number curve, also occurs with the spiral angle.

V. CONCLUSIONS

In this work we analyzed the behavior of the two most unstable modes in rotating disk flow with a stratified viscosity and compared the results with existing results for the constant viscosity case.

The main conclusions of this work may be summarized as follows:

(1) The considered viscosity profiles with $\nu(0)/\nu(\infty)>1$ reduce, in most cases, the stability of the hydrodynamic field. In the case of stationary disturbances the critical Reynolds number, based on the bulk viscosity, is strongly reduced and the unstable region is significantly enlarged. The effect of the ratio $\nu(0)/\nu(\infty)$ in the model developed in this work is, qualitatively, in agreement with the results of Barcia *et al.*[3]

(2) The neutral curves exhibit a two-mode structure. The growth rate of mode 1 is 1 order of magnitude larger than mode 2, in the respective unstable regions. In addition, the growth rate of modes 1 in stratified viscosity flows are significantly larger than in constant viscosity cases.

(3) The calculations show that the absolute minimum of the most unstable mode (mode 2) is only weakly affected by viscosity stratification, and that the other mode (mode 1), while strongly destabilized, is not the first to became unstable.

(4) The proposed hydrodynamic model, with a stratified viscosity profile, shows that in most cases the system becomes more unstable, as the thickness of the layer where the viscosity varies, increases.

ACKNOWLEDGMENTS

The authors acknowledge Professor Antônio Castelo Filho (USP-S. Carlos), who developed the numerical code using the continuation method to evaluate the neutral stability curves presented in this work. Fruitful discussions with Professor R. E. Kelly from the University of California at Los Angeles and Professor D. Walgraef from the Free University of Brussels are also acknowledged. J.P. received financial support from FAPERJ (Brazil). N.M. acknowledges financial support from CNPq (Brazil).

APPENDIX A: THE EVOLUTION EQUATIONS OF THE PERTURBED FLOW

This appendix presents the technical details related to the derivation of the eigenvalue–eigenfunction problem given by Eq. (16). Substituting the perturbed variables given by (11)–(14) in the nondimensional continuity and Navier–Stokes equations and dropping nonlinear terms we obtain

$$\frac{\tilde{v}_r}{r}+\frac{\partial\tilde{v}_r}{\partial r}+\frac{1}{r}\frac{\partial\tilde{v}_\theta}{\partial\theta}+\frac{\partial\tilde{v}_z}{\partial\xi}=0, \tag{A1}$$

$$\begin{aligned}\frac{\partial\tilde{v}_r}{\partial t}+\frac{r}{R}F\frac{\partial\tilde{v}_r}{\partial r}+\frac{G}{R}\frac{\partial\tilde{v}_r}{\partial\theta}+\frac{H}{R}\frac{\partial\tilde{v}_r}{\partial\xi}+\frac{F}{R}\tilde{v}_r-\frac{2}{R}(G+1)\tilde{v}_\theta\\ +\frac{r}{R}F'\tilde{v}_z=-\frac{\partial\tilde{p}}{\partial r}+\frac{\nu}{R}\left(\frac{\partial^2\tilde{v}_r}{\partial r^2}+\frac{1}{r^2}\frac{\partial^2\tilde{v}_r}{\partial\theta^2}+\frac{\partial^2\tilde{v}_r}{\partial\xi^2}\right.\\ \left.+\frac{1}{r}\frac{\partial\tilde{v}_r}{\partial r}-\frac{2}{r^2}\frac{\partial\tilde{v}_\theta}{\partial\theta}-\frac{\tilde{v}_r}{r^2}\right)\\ +\frac{\nu'}{R}\left(\frac{\partial\tilde{v}_z}{\partial r}+\frac{\partial\tilde{v}_r}{\partial\xi}\right),\end{aligned} \tag{A2}$$

$$\begin{aligned}\frac{\partial\tilde{v}_\theta}{\partial t}+\frac{r}{R}F\frac{\partial\tilde{v}_\theta}{\partial r}+\frac{G}{R}\frac{\partial\tilde{v}_\theta}{\partial\theta}+\frac{H}{R}\frac{\partial\tilde{v}_\theta}{\partial\xi}+\frac{F}{R}\tilde{v}_\theta+\frac{2}{R}(G+1)\tilde{v}_r\\ +\frac{r}{R}G'\tilde{v}_z=-\frac{1}{r}\frac{\partial\tilde{p}}{\partial\theta}+\frac{\nu}{R}\left(\frac{\partial^2\tilde{v}_\theta}{\partial r^2}+\frac{1}{r^2}\frac{\partial^2\tilde{v}_\theta}{\partial\theta^2}+\frac{\partial^2\tilde{v}_\theta}{\partial\xi^2}\right.\\ \left.+\frac{1}{r}\frac{\partial\tilde{v}_\theta}{\partial r}+\frac{2}{r^2}\frac{\partial\tilde{v}_r}{\partial\theta}-\frac{\tilde{v}_\theta}{r^2}\right)\\ +\frac{\nu'}{R}\left(\frac{1}{r}\frac{\partial\tilde{v}_z}{\partial\theta}+\frac{\partial\tilde{v}_\theta}{\partial\xi}\right),\end{aligned} \tag{A3}$$

$$\begin{aligned}\frac{\partial\tilde{v}_z}{\partial t}+\frac{r}{R}F\frac{\partial\tilde{v}_z}{\partial r}+\frac{G}{R}\frac{\partial\tilde{v}_z}{\partial\theta}+\frac{H}{R}\frac{\partial\tilde{v}_z}{\partial\xi}+\frac{H}{R}\tilde{v}_z\\ =-\frac{\partial\tilde{p}}{\partial\xi}+\frac{\nu}{R}\left(\frac{\partial^2\tilde{v}_z}{\partial r^2}+\frac{1}{r^2}\frac{\partial^2\tilde{v}_z}{\partial\theta^2}+\frac{\partial^2\tilde{v}_z}{\partial\xi^2}+\frac{1}{r}\frac{\partial\tilde{v}_z}{\partial r}\right)\\ +2\frac{\nu'}{R}\frac{\partial\tilde{v}_z}{\partial\xi}.\end{aligned} \tag{A4}$$

Assuming a perturbation given by Eq. (15) and introducing that form in Eqs. (A1)–(A4) we obtain

$$i\left(\alpha-\frac{i}{r}\right)f+i\frac{R}{r}\beta g+h'=0, \tag{A5}$$

$$i\left(\frac{r}{R}\alpha F+\beta G-\omega\right)f+\frac{r}{R}F'h+i\alpha\pi$$
$$=\frac{1}{R}\left(\nu f''-\nu\left(\alpha^2+\frac{R^2}{r^2}\beta^2\right)f-Ff+2(G+1)g-Hf'+i\alpha\nu'h+\nu'f'\right)$$
$$+\frac{1}{R^2}\left(i\frac{R}{r}\nu\alpha f-2\,i\frac{R^2}{r^2}\nu\beta g\right)-\frac{\nu}{Rr^2}f, \tag{A6}$$

$$i\left(\frac{r}{R}\alpha F+\beta G-\omega\right)g+\frac{r}{R}G'h+i\frac{R}{r}\beta\pi$$
$$=\frac{1}{R}\left(\nu g''-\nu\left(\alpha^2+\frac{R^2}{r^2}\beta^2\right)g-Fg-2(G+1)f-Hg'+i\frac{R}{r}\beta\nu'h+\nu'g'\right)$$
$$+\frac{1}{R^2}\left(i\frac{R}{r}\nu\alpha g+2\,i\frac{R^2}{r^2}\nu\beta f\right)-\frac{\nu}{Rr^2}g, \tag{A7}$$

$$i\left(\frac{r}{R}\alpha F+\beta G-\omega\right)h+\pi'$$
$$=\frac{1}{R}\left(\nu h''-\nu\left(\alpha^2+\frac{R^2}{r^2}\beta^2\right)h-Hh'-H'h+2\,\nu'h'\right)+\frac{i}{Rr}\nu\alpha h. \tag{A8}$$

Equations (A5)–(A8) show that perturbation variables are not, strictly speaking, separable. In order to overcome the problem it is necessary to make the parallel flow assumption, usually adopted in stability analysis of growing boundary layers, where variations of the Reynolds number in the streamwise direction are ignored. Adoption of this hypothesis in rotating disk flow[12,15,22] is made by replacing r by R in Eqs. (A5)–(A8)

$$i\left(\alpha-\frac{i}{R}\right)f+i\beta g+h'=0, \tag{A9}$$

$$i(\alpha F+\beta G-\omega)f+F'h+i\alpha\pi$$
$$=\frac{1}{R}(\nu f''-\nu\lambda^2 f-Ff+2(G+1)g-Hf'+i\alpha\nu'h+\nu'f')$$
$$+\frac{1}{R^2}(i\nu\alpha f-2\,i\nu\beta g)-\frac{\nu}{R^3}f, \tag{A10}$$

$$i(\alpha F+\beta G-\omega)g+G'h+i\beta\pi$$
$$=\frac{1}{R}(\nu g''-\nu\lambda^2 g-Fg-2(G+1)f-Hg'+i\beta\nu'h+\nu'g')$$
$$+\frac{1}{R^2}(i\nu\alpha g+2\,i\nu\beta f)-\frac{\nu}{R^3}g, \tag{A11}$$

$$i(\alpha F+\beta G-\omega)h+\pi'$$
$$=\frac{1}{R}(\nu h''-\nu\lambda^2 h-Hh'-H'h+2\,\nu'h')+\frac{i}{R^2}\nu\alpha h, \tag{A12}$$

where $\lambda^2=\alpha^2+\beta^2$. Equations (A9)–(A12) reduce to Eqs. (2.16)–(2.19) given by Malik,[24] in the case of constant viscosity fluids ($\nu=1$, $\nu'=\nu''=0$). By eliminating π, neglecting terms of order R^{-2} and defining $D^n=d^n/d\xi^n$, $\overline{\alpha}=\alpha-i/R$, $\overline{\lambda^2}=\alpha\overline{\alpha}+\beta^2$, and $\eta=\alpha g-\beta f$ we obtain a sixth order system of two coupled equations in the form

$$(i\nu(D^2-\lambda^2)(D^2-\overline{\lambda^2})+i\nu'D(2D^2-\lambda^2-\overline{\lambda^2})+i\nu''(D^2+\overline{\lambda^2})+R(\alpha F+\beta G-\omega)(D^2-\overline{\lambda^2})-R(\overline{\alpha}F''+\beta G'')$$
$$-iHD(D^2-\overline{\lambda^2})-iH'(D^2-\overline{\lambda^2})-iFD^2)h+(2(G+1)D+2G')\eta=0, \tag{A13}$$

$$(2(G+1)D-iR(\alpha G'-\beta F'))h+(i\nu(D^2-\lambda^2)+i\nu'D+R(\alpha F+\beta G-\omega)-iHD-iF)\eta=0. \tag{A14}$$

Equations (A13)–(A14) reduce to Eqs. (2.20)–(2.21) given by Malik,[24] in the case of constant viscosity fluids and may be rewritten in the form of Eq. (16).

APPENDIX B: NUMERICAL PROCEDURE

Building the neutral curves requires finding the set of points $c(s)=(\alpha(s),\beta(s),R(s))$ that satisfy $F(c(s))=0$, where $F:R^3->R^2$ is given by $F=(\mathcal{I}(\omega),\mathcal{R}(\omega)-\omega_r)^T$. The neutral curves are built using a predictor–corrector continuation method described by Allgower and Georg.[23] Here, for completeness, we will give a short description of the employed method.

(1) The perturbation frequency ω_r is specified and an initial point c_0, in the parameters space α,β,R is given. This point is not necessarily on the neutral curve.

(2) This initial point is corrected using an inexact Newton iteration given by

$$c_i^{n+1}=c_i^n-F'(c_i^0)^+F(c_i^n), \tag{B1}$$

where $F'(v_0)^+$ is the pseudoinverse of Moore–Penrose of the Jacobian of F. The Jacobian is computed numerically, using a finite difference approximation.

(3) To obtain an initial estimate of the next point over the curve, a predictor step is employed, based on the first order Euler method

$$c_{i+1}^0 = c_i + h\, t(F'(c_i)), \tag{B2}$$

where h is a suitable step size, and $t(F'(c_i))$ is the tangent vector to curve $c(s)$.

(4) The value c_{i+1}^0 is corrected in a corrector step using Eq. (B1) iteratively until a satisfactorily converged value is obtained.

(5) The generalized eigenvalue/eigenfunction problem required to evaluate $F(c(s))$ is solved numerically, using an inverse power method double precision routine for complex generalized nonsymmetric eigenproblems, that takes advantage of the sparsity of the coefficient matrices.

[1] V. G. Levich, *Physicochemical Hydrodynamics* (Prentice Hall, Englewood Cliffs, NJ, 1962).
[2] J. S. Newman, *Electrochemical Systems*, 2nd ed. (Prentice Hall, Englewood Cliffs, NJ, 1991).
[3] O. E. Barcia, O. R. Mattos, and B. Tribollet, "Anodic dissolution of iron in acid sulfate under mass transport control," J. Electrochem. Soc. **139**, 446 (1992).
[4] J. R. R. M. Ferreira, O. E. Barcia, and B. Tribollet, "Iron dissolution under mass transport control: The effect of viscosity on the current oscillation," Electrochim. Acta **39**, 933 (1994).
[5] I. Epelboin, G. Gabrielli, M. Keddam, J. C. Lestrach, and H. Takenouti, "Passivation of iron in sulfuric acid medium," J. Electrochem. Soc. **126**, 1632 (1979).
[6] P. Russel and J. Newman, "Current oscillations observed within the limiting current plateau for iron in sulfuric acid," J. Electrochem. Soc. **133**, 2093 (1986).
[7] B. Tribollet and J. Newman, "The modulated flow at a rotating disk electrode," J. Electrochem. Soc. **130**, 2016 (1983).
[8] A. B. Geraldo, O. E. Barcia, O. R. Mattos, F. Huet, and B. Tribollet, "New results concerning the oscillations observed for the system iron-sulphuric acid," Electrochim. Acta **44**, 455 (1998).
[9] N. Smith, "Exploratory investigation of laminar boundary layer oscillations on a rotating disk," Technical Rep. No. TN-1227, NACA, December 1946.
[10] N. Gregory, J. T. Stuart, and W. S. Walker, "On the stability of three-dimensional boundary layers with application to the flow due to a rotating disk," Philos. Trans. R. Soc. London, Ser. A **248**, 155 (1955).
[11] D. T. Chin and M. Litt, "An electrochemical study of flow instability on a rotating disk," J. Fluid Mech. **54**, 613 (1972).
[12] S. Wilkinson and M. R. Malik, "Stability experiments in the flow over a rotating disk," AIAA J. **23**, 588 (1985).
[13] H. L. Reed and W. S. Saric, "Stability of three-dimensional boundary layers," Annu. Rev. Fluid Mech. **21**, 235 (1989).
[14] A. J. Faller, "Instability and transition of the disturbed flow over a rotating disk," J. Fluid Mech. **230**, 245 (1991).
[15] R. J. Lingwood, "Absolute instability of the boundary layer on a rotating disk," J. Fluid Mech. **299**, 17 (1995).
[16] H. Schlichting and K. Gersten, *Boundary Layer Theory* (Springer, Berlin, 1999).
[17] P. Schäfer, J. Severin, and H. Herwin, "The effect of heat transfer on the stability of laminar boundary layers," Int. J. Heat Mass Transfer **38**, 1855 (1995).
[18] M. Turkyilmazoglu, J. W. Cole, and J. S. B. Gajjar, "Absolute and convective instabilities in the compressible boundary layer on a rotating disk," CLSCM Rep. No. CLSCM-1998-001, University of Manchester, 1998.
[19] P. Huerre and P. A. Monkewitz, "Absolute and convective instabilities in free shear layers," J. Fluid Mech. **159**, 151 (1985).
[20] T. von Kármán and Z. Angew, "Uber Laminare und Turbulente Reibung," Math. Mec. **1**, 233 (1921).
[21] S. Calabrese Barton and A. C. West, "Electrohydrodynamic impedance in the presence of nonuniform transport properties," J. Electrochem. Soc. **148**, A381 (2001).
[22] M. R. Malik, S. Wilkinson, and S. A. Orzag, "Instability and transition in a rotating disk," AIAA J. **19**, 1131 (1981).
[23] E. Allgower and K. Georg, *Continuation Methods—An Introduction* (Springer, New York, 1990).
[24] M. R. Malik, "The neutral curve for stationary disturbances in rotating disk flow," J. Fluid Mech. **164**, 275 (1986).